

Circuits for a Cubic-Millimeter Energy-Autonomous Wireless Intraocular Pressure Monitor

Mohammad Hassan Ghaed, Gregory Chen, Razi-ul Haque, Michael Wieckowski, Yejoong Kim, Gyouho Kim, Yoonmyung Lee, Inhee Lee, David Fick, Daeyeon Kim, Mingoo Seok, Kensall D. Wise, *Fellow, IEEE*, David Blaauw, *Fellow, IEEE*, and Dennis Sylvester, *Fellow, IEEE*

Abstract—Circuit blocks for a 1.5 mm^3 microsystem enable continuous monitoring of intraocular pressure. Due to power and form-factor limitations, circuit blocks are designed at nanowatt power levels not completely explored before. The system includes a 75% efficient 90 nW DC-DC converter which is the most efficient reported sub- μW converter in literature. It also includes a novel 4.7 nJ/bit FSK radio that achieves 10 cm of transmission range at 10^{-6} BER which is also the lowest number reported for short-range through-tissue wireless links for biomedical implants. A MEMS capacitive sensor and $\Sigma\Delta$ capacitance-to-digital converter measure IOP with 0.5 mmHg accuracy. A microcontroller processes and saves IOP data and stores it in a 2.4 fW/bitcell SRAM. The microsystem harvests a maximum power of 80 nW in sunlight with a light irradiance of $100 \text{ mW}/\text{cm}^2$ AM 1.5 from an integrated 0.07 mm^2 solar cell to recharge a 1 mm^2 $1 \mu\text{Ah}$ thin-film battery and power the load circuits. The design achieves zero-net-energy operation with 1.5 hours of sunlight or 10 hours of bright indoor lighting daily.

Index Terms—Biomedical monitoring, CMOS memory integrated circuits, digital signal processors, photovoltaic power systems, radio transceivers, sensor systems.

I. INTRODUCTION AND APPLICATION DESCRIPTION

ULTRA-LOW power microsystems have become possible today due to advances in low-power integrated circuit design, improvements in fabrication technology, and the evolution of more efficient low-profile energy sources. Many biomedical applications can benefit from such microsystems. In this paper, we focus on circuits for one specific application, continuous intraocular pressure sensing for glaucoma diagnosis and management. Glaucoma is the second-leading cause of blindness, affecting over 60 million people worldwide and is predicted to impact nearly 80 million by 2020 [1]. The ophthalmological community recognizes the benefits and challenges of con-

Manuscript received December 06, 2012; revised March 19, 2013; accepted April 10, 2013. Date of publication August 23, 2013; date of current version November 21, 2013. This paper was recommended by Associate Editor J. M. de la Rosa.

M. H. Ghaed (corresponding author), R.-U. Haque, Y. Kim, G. Kim, Y. Lee, I. Lee, D. Fick, K. D. Wise, D. Blaauw, and D. Sylvester are with the University of Michigan, Ann Arbor, MI 48105 USA (e-mail: ghaed@umich.edu).

G. Chen was with the University of Michigan, Ann Arbor, MI 48105 USA. He is now with Intel Corp., Hillsboro, OR 97124 USA (e-mail: grgchen@umich.edu).

M. Wieckowski was with the University of Michigan, Ann Arbor, MI 48105, USA. He is now with Mala Geosciences, Charleston, SC 29492 USA (e-mail: wieckows@umich.edu).

M. Seok was with the University of Michigan, Ann Arbor, MI 48105 USA. He is now with Columbia University, New York, NY 10027 USA (e-mail: ms4415@columbia.edu).

D. Kim is with Advanced Design Group, Logic Technology Development, Intel Corporation, Hillsboro, OR 94124 USA.

Color versions of one or more of the figures in this paper are available online at <http://ieeexplore.ieee.org>.

Digital Object Identifier 10.1109/TCSI.2013.2265973

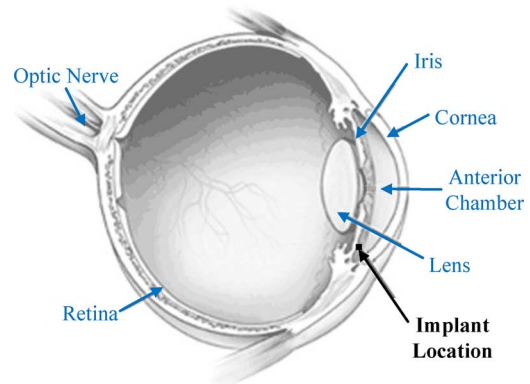


Fig. 1. The 1.5 mm^3 IOP monitor is implanted in the anterior chamber of the eye as part of a treatment for glaucoma.

tinuous IOP monitoring, motivating previous work in this area [2]–[6]. A contact lens approach measures IOP by measuring the deformation of the cornea curvature due to IOP changes [7]. This reduces patient intervention, but requires an external power source from an eye patch surrounding the eye of the patient. Typical usage is limited to a 24 hour time period. Another recent implanted solution stores energy on a $24 \mu\text{F}$ capacitor array to continuously collect data over a 24 hour period, but requires a 27 mm antenna for data and power transfer [8].

One primary factor that distinguishes the proposed intraocular pressure sensing microsystem (IOPM) from previous work is its small 1.5 mm^3 form factor that enables us to implant it in the anterior chamber of the eye (Fig. 1). From a circuit perspective, the major challenge is to design all the system components shown in Figs. 2 and 3 such that they do not exceed the power budget of the system. Table I shows the main circuit-level limitations on the system. In order to realize these goals we introduce novel blocks with record-low energy consumption and apply analog and digital low-power techniques to other blocks to keep average and peak power consumption below the values dictated by the small thin-film battery.

As shown in Fig. 3, the monitor contains two integrated circuit (IC) chips fabricated in a $0.18 \mu\text{m}$ CMOS process. The top IC contains a solar cell and fully-integrated wireless transceiver (TRx). The bottom IC contains a sigma-delta capacitance to digital converter ($\Sigma\Delta$ CDC), microprocessor (μP), and static random access memory (SRAM). The solar cell and a thin-film solid-state Li battery deliver power to the microsystem through the power management units (PMU), allowing microsystem operation without patient intervention for power delivery. Ambient light is used for energy harvesting, and wireless communication signals easily penetrate the package to form a bidirectional interface with the outside world. A $2 \text{ mm} \times 1.5 \text{ mm}$

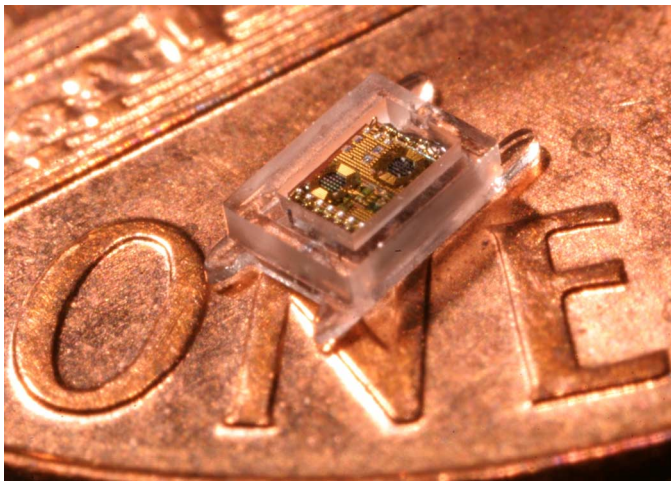
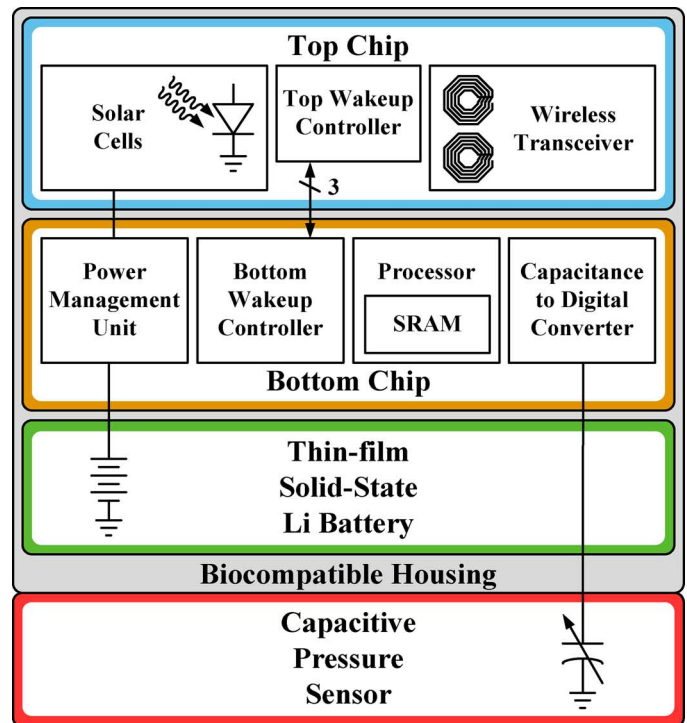


Fig. 2. IOP monitor microsystem photo and diagram. The top of the glass enclosure is omitted in the photo to highlight circuit components.



MEMS capacitive sensor forms the bottom layer as shown in Fig. 3 [9]. All these blocks are encapsulated in a sealed glass container. The biocompatibility of the glass container has been demonstrated through implantation and in-vivo measurements in the eye [10]–[12].

Section II describes a $\Sigma\Delta$ CDC that achieves $2 \times$ sensitivity improvement over previous IOP monitors [13]. Section III describes the design of an ultra-low-power 8-bit microcontroller and SRAM which achieve the lowest average power to date. Section IV explains the novel dual-resonator FSK transceiver that enables us to achieve 10 cm of through-tissue transmission at an energy consumption of 4.7 nJ/bit. Section V covers the design of the switched capacitor circuit that is, to authors’ best knowledge, the most efficient sub- μ W DC-DC converter to date. Finally, Section V draws the conclusion of the paper.

II. CAPACITANCE TO DIGITAL CONVERTER

A. Capacitance to Digital Converter Background

Capacitance to digital converters (CDCs) apply an excitation force to a variable sensor capacitance to generate a voltage, current, or time and then use analog to digital (ADC) techniques to output a digital value. Simple readout circuitry charges and discharges the capacitance at one node of a CMOS ring oscillator, and measures the oscillation frequency. However, this method is highly dependent on process, voltage and temperature variations. A 500 μ W capacitance to digital converter design incorporates the sensor capacitance into the digital to analog converter portion of a successive approximation register (SAR) ADC [14]. SAR ADCs have been demonstrated with figures of merit as low as 4.4 fJ/conversion step in a 1.9 μ W design [15]. Several capacitance to digital converter designs incorporate the sensor capacitance as a switched-capacitor resistor in an integrating amplifier to achieve accuracies within 19.3 aF [16]–[18]. The slope of the integrator output is proportional to the pressure sensor capacitance. The integrator output ramp can be digitized using $\Sigma\Delta$ or pulse-position modulation (PPM) ADCs, with a demonstrated 5.6 μ W $\Sigma\Delta$ ADC achieving 303 fJ/conversion step [19] and a 14 μ W PPM ADC achieving 98 fJ/conversion step [20].

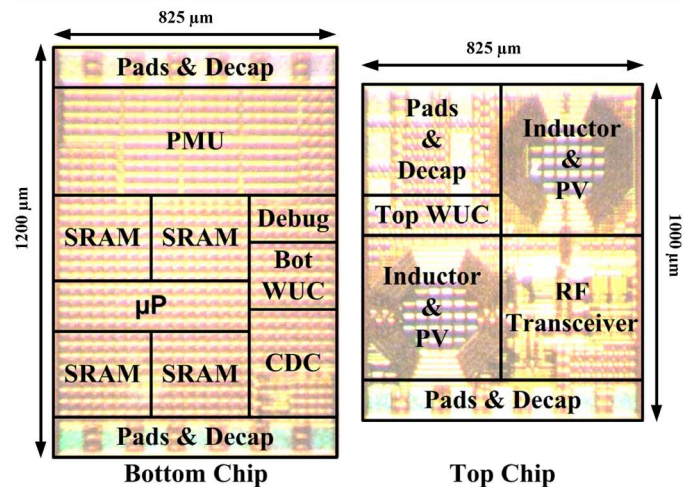


Fig. 3. IOP monitor block diagram and die photos.

TABLE I
CIRCUIT CONSTRAINTS ON IOPM

Module	Requirement	Achieved
CDC Sensitivity	1mmHg	0.5mmHg
CDC Active Power	10 μ W	7 μ W
Radio Energy/bit	7 nJ/bit	4.7 nJ/bit
Total Stand-by Power	5nW	3.3nW
Total Silicon Area Including Decap, TRx Coils, and Pads	1.8mm ²	1.8mm ²

B. Capacitance to Digital Converter Implementation

The capacitance to digital converter for the IOP sensor is designed to achieve low sensitivity to process variation, voltage fluctuations, and clock uncertainty with low peak and average power. Precision is improved using differential measurements with common voltage and frequency references. 7.0 μ W active

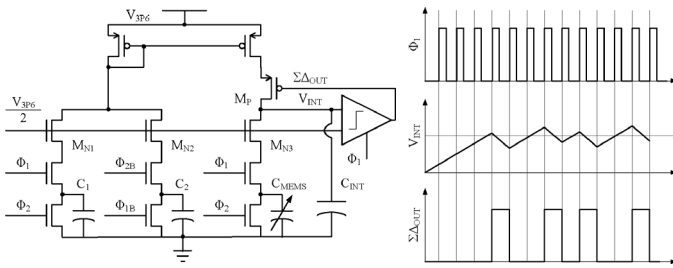


Fig. 4. The capacitance to digital converter generates a pressure-sensitive current by switching the pressure sensor and measures the pressure sensor capacitance with $\Sigma\Delta$ modulation.

power is achieved by generating small excitation currents using weakly inverted devices and eliminating integrating amplifiers found in typical $\Sigma\Delta$ converters.

The CDC measures the capacitance of the pressure sensor (C_{MEMS}) by differentially comparing it to 250 fF fixed MIM capacitors (C_1, C_2) (Fig. 4). The capacitors are used to generate pressure-sensitive and fixed currents by using them as switched-capacitors and then applying a fixed voltage across them. These difference of the pressure sensitive and the $\Sigma\Delta$ modulated fixed current is accumulated onto an integration capacitor (C_{INT}). The fixed current is duty cycled to regulate the voltage on C_{INT} at $V_{3P6}/2$. The voltage on C_{INT} (V_{INT}) is compared with $V_{3P6}/2$ using a clocked comparator and device M_{P1} is modulated with $\Sigma\Delta_{OUT}$ to control V_{INT} . $\Sigma\Delta_{OUT}$ is accumulated into a 14 b digital value with a 10,000:1 decimation filter that counts the number of cycles where $\Sigma\Delta_{OUT}$ is high over a 10,000 clock cycle period to generate the digital measurement of sensor capacitance.

$\Sigma\Delta$ modulation cancels out quantization and temporal noise and also devices and references are carefully matched allowing higher accuracy with lower power circuits. The capacitors are switched using a shared 50 kHz clock to reduce clock sensitivity. C_1 and C_2 use 180° out of phase clocks (Φ_1, Φ_2) to create a more-constant fixed impedance, yielding better results than switching a single 500 fF MIM capacitor. A fixed voltage is dropped across the switched-capacitor resistors to generate both a pressure-sensitive and a fixed current. This voltage drop is regulated with saturated transistors M_{N1}, M_{N2} , and M_{N3} . A reference voltage equal to $V_{3P6}/2$ is generated using a 2:1 switched capacitor divider and connected to the gate of the current limiting devices. Since $V_{3P6}/2$ is shared, the capacitance to digital converter output also has reduced sensitivity to V_{3P6} .

Low power techniques are carefully applied in the CDC to decrease overall IOP energy usage and reduce the amount of harvested energy required for energy autonomy. A 50 kHz ring-oscillator-based clock is chosen to satisfy CDC power requirement in Table I. This requirement comes from the maximum continuous current the thin-film battery can supply before its voltage drops more than 100 mV. The microsystem's battery can supply at most $40 \mu\text{W}$, so to reduce power the capacitance to digital converter generates a 0.9 V 50 kHz clock with a current-starved ring oscillator, and then converts it to a 3.6 V clock for the switched capacitor resistors and comparator. The slow clock saves power by decreasing the pressure-sensitive and fixed currents and also reducing the activity and power of the comparator. However, since capacitance to digital converter accuracy is related to the number of clock cycles, using a slower clock does not reduce the energy per measurement. Energy per

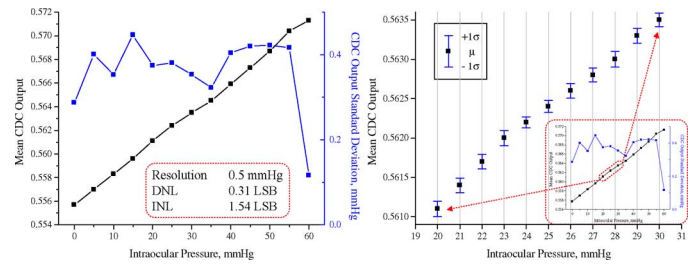


Fig. 5. The pressure sensor and capacitance to digital converter achieve 0.5 mmHg IOP accuracy with high linearity.

measurement is inversely related to clock frequency because of increased leakage energy over a longer measurement time period. Static current is decreased by using an integration method that does not require an amplifier, avoiding the power overhead for its quiescent current. Between pressure measurements, the clock is disabled and only leakage power is consumed. To reduce leakage power, all transistors in the capacitance to digital converter are ultra high threshold voltage, thick-gate oxide (UVT) devices with leakage power that is three orders of magnitude lower than logic device leakage.

C. Capacitance to Digital Converter Measurement Results

The MEMS capacitive pressure sensor is placed in a pressure chamber and connected to the capacitance to digital converter for measurement. The pressure range of interest for IOP measurements is 0–60 mmHg above atmospheric pressure, with healthy IOP ranging between 10–21 mmHg. Higher pressures can indicate glaucoma [21]. The pressure sensor has a resolution of 26 fF/mmHg [22]. Pressure sensor hysteresis effects contribute 1 mmHg of uncertainty to the pressure measurement. Goldmann applanation is the golden standard for IOP measurements and achieves 1 mmHg accuracy. The capacitance to digital converter has 0.5 mmHg accuracy, which translates to 13 fF, while consuming $7.0 \mu\text{W}$ active and 173 pW standby power (Fig. 5). The standard deviation is less than 0.5 mmHg with 50 measurements taken at each pressure. The output is highly linear due to the contact-mode pressure sensor and switched-capacitor capacitance to digital converter techniques. The differential non-linearity (DNL) is 0.31 LSB and the integrated non-linearity (INL) is 1.54 LSB, calculated using end point linear calibration which were within the range of expected results based on simulations across process corners.

Although body temperature is well controlled, the outer eye does experience some temperature fluctuations on the order of 10°C [23]. To reduce temperature sensitivity, the capacitive sensor is sealed in vacuum to mitigate the effects of thermal expansion. The fixed MIM capacitors in the capacitance to digital converter also exhibit low temperature dependence. The temperature sensitivity of the capacitance to digital converter is $5.6 \text{ mmHg}/^\circ\text{C}$ as shown in Fig. 6(b). From [23], we expect the temperature at the surface of the iris to vary between 15°C and 40°C in extreme external environments. This error due to temperature variations would need to be calibrated out with an external temperature measurement. This measurement can be done by adding a sub- μW temperature sensing module similar to [24] to IOPM. Measurements of the pressure sensor used in this work indicate drift of less than 0.5 mmHg over the course of 2 weeks, which is most likely due to mechanical wearing of sensor membrane under pressure. Long-term in vivo sensor drift

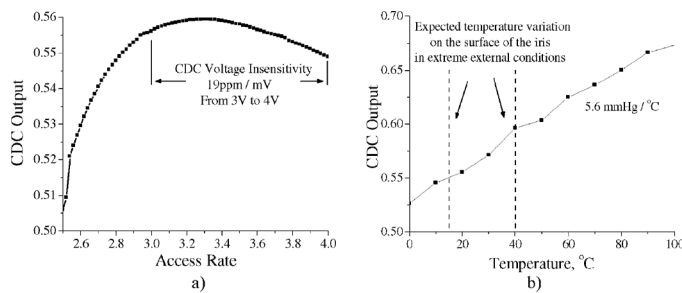


Fig. 6. Pressure measurement sensitivity to variations in a) battery voltage and b) temperature.

studies would be useful in assessing the impact of scar tissue build-up on the sensor on IOP measurements.

III. MICROPROCESSOR AND MEMORY

A. Microprocessor and SRAM Background

There has been significant previous work on low-power microprocessors and SRAM [25]. V_{DD} scaling reduces dynamic energy quadratically and leakage power exponentially. However, delay degrades resulting in increased leakage energy per microprocessor instruction. The competing trends in dynamic and leakage energy lead to an intermediate near-threshold or sub-threshold V_{DD} where total energy per instruction is minimized [25]–[28]. Numerous designs have applied V_{DD} scaling to custom and commercial microprocessors to achieve energy as low as 2 pJ per instruction [29], [30]. To ensure low- V_{DD} functionality, previous works remove high fan-in standard cells and perform extensive Monte Carlo analysis of sequential elements [29], [31]. When inactive, the microprocessor consumes only leakage power. Optimal technology selection balances active and standby energy for the microprocessor based on its duty cycle [32]. Power gate size should be chosen to minimize leakage while meeting performance requirements, which are often loose in ultra-low power sensor applications [31]. The power gate can be implemented as a low-leakage UVT device and then overdriven with V_{BATT} to maximize on-to-off current ratio [33].

Processor data can be stored in volatile or non-volatile memories. Non-volatile memories such as embedded Flash do not require power to retain data, making them good candidates for reducing standby mode power [34]. However, these memories have high write powers, require high write voltages, and are not readily available to academic researchers. SRAM is easily designed in CMOS processes using only the nominal voltage. However, data retentive SRAM cannot be power gated without data loss, so minimizing SRAM leakage is vital for achieving energy-autonomy. V_{DD} scaling in SRAM reduces energy but degrades stability margins [35]. An 8T SRAM bitcell separates read and write constraints to improve stability [36], [37]. A 10T SRAM approach further improves read stability by pulling up read bitlines (BLs) and reducing read buffer leakage [38], [39]. The IOP microsystem includes a 9.8 pW 0.45 V 4 kb ultra-low-leakage 10T SRAM. The SRAM bitcell uses UVT devices and gate length biasing in the data-retaining portion while power gating the read buffer to achieve 2.4 fW/bit standby leakage [40]. The SRAM drives the BLs at 0.9 V to improve write stability, and employs PMOS pass gates because they are

faster at the V_{DD} of interest and hierarchical BLs to reduce latency.

B. Microprocessor and SRAM Implementation

The microprocessor coordinates data transfer and management among the capacitance to digital converter, wireless transceiver, and SRAM. After a capacitance to digital converter measurement is complete, the microprocessor wakes up from standby mode and reads the result from a memory mapped location. The microprocessor can perform digital signal processing (DSP) to extract useful medical information from raw IOP data as well as perform data compression. Simple examples of DSP include detection of the average, peak, or changes in IOP over a time interval. This analysis is facilitated by the linear relationship between pressure and capacitance to digital converter output. The microprocessor can also be used to compress IOP data, reducing memory footprint. The full-range capacitance to digital converter output ranges from 0–10 000 with a 14 b digital representation. However, over the pressures of interest, the output range is 180 allowing the microprocessor to compress the data to an 8 b value. Storing differential instead of absolute IOP values further reduces memory footprint, enabling leakage reductions through power gating of unused SRAM banks during standby mode. After processing the data is stored into SRAM. When the user generates a wireless wakeup event, a separate microprocessor program is called. This program receives wakeup signals from the transceiver, retrieves data from SRAM, and initiates wireless transmissions.

Low-power techniques in the microprocessor and SRAM reduce active mode peak power and standby-mode-limited energy consumption. The microprocessor is an 8 b microcontroller with an instruction set that supports 16 registers. In the 8 b instruction, 4 bits are an instruction operand. For 15 operands, the other 4 instruction bits denote a register. These instructions compute operations between the designated register and a general purpose register that is used in every instruction. The 16TH operand performs special tasks based such as initiating a transceiver transmission and entering standby mode. V_{DD} is scaled near the minimum energy point, thus, μP and SRAM consume 90 nW at 0.45 V. In standby mode, an NMOS UVT header transistor virtually eliminates the microprocessor's contribution to standby mode power. In active mode, this header is overdriven with V_{BATT} to meet the 100 kHz performance target.

IV. WIRELESS TRANSCIVER

A. Transceiver Background

Wireless transceivers for medical implants are limited by antenna size and power budget constraints. Passive backscattering techniques bypass transmitter power budget limitations by reflecting an incoming RF signal using impedance modulation. These techniques achieve a 10^{-6} transmit bit error rate (BER) over a 2 cm transmission channel with a 3.5 cm diameter coil [41] and a 1.5×10^{-6} BER over 15 mm with a 40 mm coil [42]. However, these devices are too large for IOP monitoring. Active techniques draw from microsensor power supplies to achieve higher transmit performance with smaller antennas or coils. These transmitters achieve energy efficiencies as low as 20.4 nJ/bit with coils as small as 0.47 mm [8], [43]–[46]. Previous transceiver implementations consume higher peak

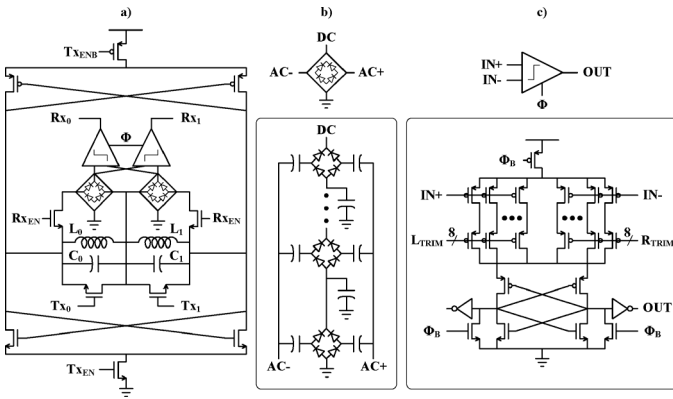


Fig. 7. (a) The transceiver uses a dual-resonator with a combined local oscillator and power amplifier. (b) The multi-stage rectifier. (c) The variable offset comparator.

power than the 1 mm^2 battery can source and limit device lifetime because of high leakages.

B. Transceiver Implementation

The fully-integrated transceiver receives wireless wakeup signals and responds with IOP data. It uses FSK modulation with two tones at 433 MHz and 915 MHz in the industrial, scientific, and medical (ISM) bands. The doctor or patient places an external wand over the eye and transmits a wireless wakeup signal to activate the IOP monitor. The receiver is activated (R_{XEN}) and generates one of two digital signals (R_{X0} , R_{X1}) based on the wakeup signal frequency (Fig. 7). The wakeup signal is coupled onto one LC tank of the dual-resonator structure and connected to the rectifier with a switch controlled by R_{XEN} . The ac signal is converted to dc using one of two 8-stage full-bridge rectifiers. The dc offset is then converted to the digital R_{X0} and R_{X1} signals by comparing the dc outputs of the rectifiers with two 50 Hz variable-offset comparators. Thus, the R_{X0} or R_{X1} is generated when more RF energy is received on either half of the dual-resonator tank than the other, indicating a wakeup signal at the intended frequency. These digital signals are sent to the top wakeup controller (top WUC), which coordinates communication with the microprocessor. The microprocessor receives signals from the top wakeup controller and responds by issuing commands to the top wakeup controller. The top wakeup controller determines what data to transmit (T_{X0} , T_{X1}) and enables the transmitter (T_{XEN}) to send medical data to the external wand.

The transceiver uses a dual-resonator LC tank [47]. The dual-resonator allows higher frequency separation between the FSK tones compared to a single LC tank using a varactor. Using two separate bands completely eliminates the overlap between their phase noise skirts, thus relaxing oscillator phase noise requirements. It is formed by the series connection of two LC tanks (L_0C_0 , L_1C_1) that are tuned to 433 MHz and 915 MHz. It resonates when a wireless signal at either of these frequencies is sent to the IOP monitor, with the ac signal developed across the corresponding LC tank. Therefore, the receiver can detect two wakeup signals to initiate separate microprocessor procedures or program the IOP monitor. Differential analysis of the received ac signals reduces the false wakeup rate from noise

outside of the resonance frequencies because those frequencies generate a common mode at the comparator input. Most importantly, DC outputs of the rectifiers, are cancelled out during this process. The dual-resonator transmits data by shorting one LC tank, enabling the oscillator, and radiating power from the inductor coils. It achieves high tone separation with 10% lower circuit area than two separate LC oscillators.

Wireless wakeup signals are detected by rectifying ac signals that are coupled onto the dual resonator. The ac signals are converted to a dc voltage using 8 full-bridge rectifier stages. Each half of the dual resonator is ac coupled to each of its associated rectifier stages, where Schottky diodes generate a dc potential. The Schottky rectifier is passive and has a smaller forward-bias voltage than diode-connected MOS transistors (200 mV vs. 450 mV for HVT NMOS devices in this technology), making it a suitable choice for this application. The passive nature of the Schottky rectifier enables us to cascade 8 stages to achieve a higher DC output without consuming the limited energy available to IOPM. The tradeoff in adding multiple stages is an increased output rise time from 80 μs (single stage) to 1.2 ms (8-stage), which is not important in this application as the external wakeup device will be held close to the IOPM for several seconds during transmission. The output of the 8-stage rectifier is converted to a full swing digital signal using a clocked comparator. This comparator runs continuously in standby mode, so it must be low power to meet the microsystem's energy budget. The comparator runs with a 31 pW 50 Hz clock that is generated at 0.45 V using a leakage-based oscillator [48] and then level-converted to the 3.6 V comparator input.

The transmitter uses an architecture that combines the local oscillator (LO) and power amplifier (PA). This modification is necessary to reduce circuit area by including fewer fully-integrated inductors. For PA functionality, the inductors need to be large to radiate enough power for the external wand to detect. However, the 0.41 mm diameter, 5-turn coils degrade LO phase noise because of low quality factor (Q). The Q of the inductors is further degraded by placing solar cells underneath the coil openings to save area. Based on 3D EM simulation results, inductor Q is reduced from 11 to 9.5 at 433 MHz, and from 12.3 to 10.6 at 915 MHz when solar cells were added. The effects of lower Q on phase noise are mitigated by using the dual-resonator with high frequency separation between tones.

During data transmission, the transceiver requires greater peak power than the battery can supply. Therefore the transceiver draws instantaneous power from a local charge reservoir. The local charge storage is implemented as 1.6 nF of integrated metal oxide semiconductor (MOS) and MIM capacitance on the ICs. The MIM density is $2 \text{ ff}/\mu\text{m}^2$ in this technology. The 1.6 nF value was the maximum amount of capacitance that could fit on silicon without violating our area constraint in Table I. The transceiver sends a single 100 ns pulse at a time, which degrades the voltage on the local supply by less than 25%. The local supply is then recharged for the next 131 μs from the battery, using a resistor to prevent high currents from damaging the battery, resulting in an effective data rate of 7.5 kb/sec (Fig. 8). Low-leakage IO devices with reduced sizes limit leakage power while meeting performance targets. The transmitter can send daily IOP data taken every 15 minutes in 130 ms.

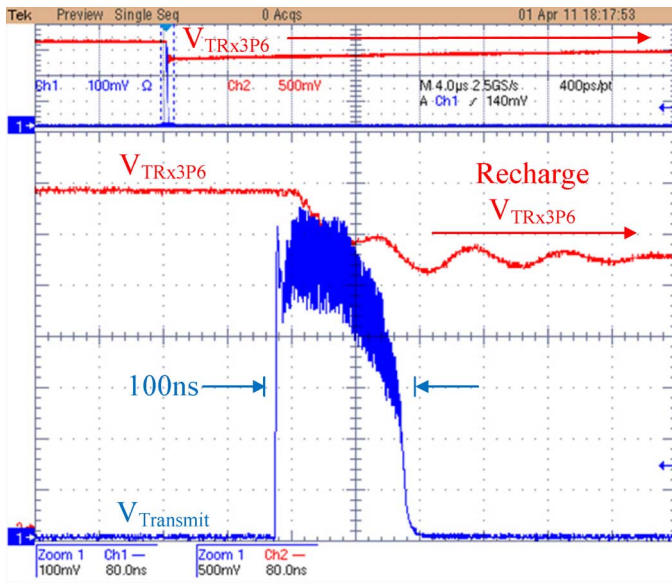


Fig. 8. Data transmissions are sent in 100 ns pulses because of peak power constraints.

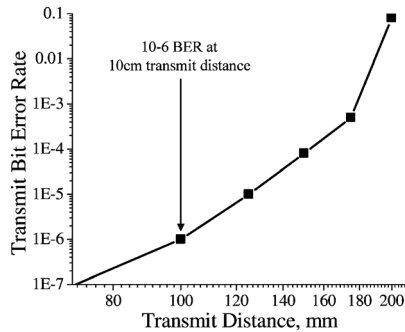


Fig. 9. Transmitter BER plot.

C. Transceiver Measured Results

The transceiver is tested in a laboratory using an external wand to communicate with the IOPM. The wand contains PCB-trace inductors and matching networks connected to an RF signal generator and spectrum analyzer to transmit and receive data [49]. The transmit media between the IOP monitor and wand is air as well as 0.5 mm of saline to model the aqueous humor and cornea. The IOP monitor is demonstrated to wake up when a 1 W wireless signal is sent at a distance of 4 mm. After receiving this signal, the IOP monitor will respond by transmitting data to the wand with a BER of 10^{-6} at a distance of 10 cm. The transmit BER vs. transmission distance is shown in Fig. 9.

In order to demonstrate in vivo system operation, the radio was implanted in a mouse as shown in Fig. 10(a). The external wand [shown in Fig. 10(b)] receives the signal using a PCB coil. The received signal is amplified, filtered, and down-converted using a spectrum analyzer to reconstruct the transmitted waveform. Fig. 10(c) shows the successful reception of transmitted data in the implanted system.

V. POWER MANAGEMENT AND ENERGY AUTONOMY

A. Power Management Unit Background

Efficient energy harvesting and voltage regulation is necessary for energy-autonomous operation. Environmental energy

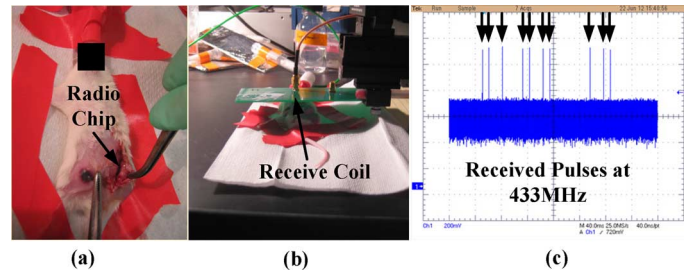


Fig. 10. (a) In-vivo radio testing implantation. (b) Measurement setup. (c) Received pulses at 433 MHz.

is sporadic and must be stored on a secondary supply for continuous power. Solar cells output below 500 mV [50] and secondary supplies commonly have higher voltages because of energy density or battery chemistry constraints, requiring dc-dc voltage conversion. Converter efficiency degrades at low loads because overheads do not scale down proportionally to delivered power. A low-power energy harvesting boost converter demonstrates 80% efficiency with a $100 \mu\text{W}$ harvester and 45% at $1 \mu\text{W}$ [51]. However, boost converters require large external inductors that do not meet the IOPM volume constraints. Switched capacitor voltage harvesters can be designed to perform dc-dc conversion using integrated capacitors. Harvesting switched capacitor networks achieve 84% efficiency at 1 mW [52] and 40% at 958 nW [33].

Energy stored on the secondary battery must be converted to the load circuit voltage levels. A buck-converter demonstrates 80% efficiency at a $1 \mu\text{W}$ load [53]. As with energy harvesting boost converters, buck-converters require external inductors which are too large for the IOP monitor, and switched capacitor voltage regulators achieve similar functionality with integrated capacitors. A down-converting switched capacitor voltage regulator achieves approximately 76% efficiency at a $100 \mu\text{W}$ load and 60% at $1 \mu\text{W}$ [29]. Linear regulators exhibit high line regulation and low output noise, but suffer from poor efficiencies at high conversion ratios and cannot be reused for energy harvesting. Hybrid switched capacitor plus linear regulator systems increase efficiency by reducing linear regulator dropout in systems with high conversion ratios. Hybrid dc-dc converters demonstrate efficiencies of 55% at 126 nW [48] and 18% at 100 pW [33].

B. Power Management Unit Implementation

The power management unit recharges the battery from the solar cell and delivers power to load circuits (Fig. 11). The same switched cap voltage regulator (SCVR) that up-converts solar cell voltage to battery voltage is re-used to down-convert battery voltage and supply CMOS circuits. The solar cell size is limited to 0.07 mm^2 by the size restrictions of the monitor and is fabricated in an unmodified CMOS process, i.e., without any extra fabrication steps, using the deep n-well to p-well and p-well to n-active diodes. It is located underneath the transparent transceiver coil openings to save area. The output of the solar cell (V_{SOLAR}) connects to the V_{OP45} node of the switched capacitor voltage regulator. When V_{SOLAR} exceeds 450 mV, the 0.32 mm^2 8:1 voltage regulator up-converts the harvested energy to above 3.6 V and recharges the battery. The thin-film solid-state Li battery is supplied by Cymbet Corporation and uses a commercial chemistry, but its size is tailored specifically for this application [54]. This tailoring is necessary since most commercial

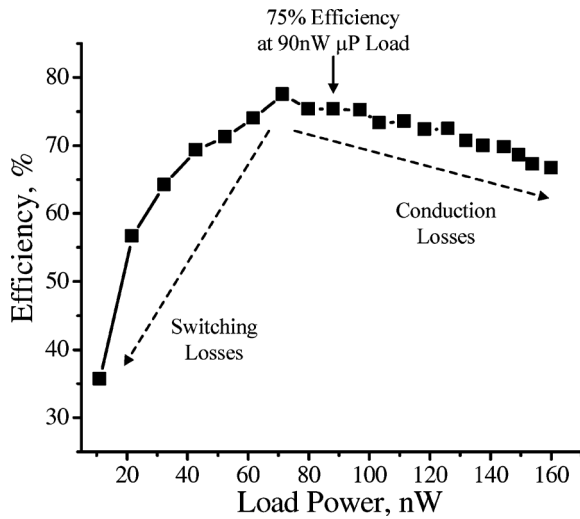


Fig. 13. The switched capacitor voltage regulator is optimized for low switching and conduction losses to achieve 75% efficiency.

TABLE II
POWER BREAKDOWN FOR THE IOPM

Active Mode	Power	Time/Day	Energy/Day
CDC	7.0 μ W	19.2 s	134.8 μ J
TRx	47.0 mW	134.4 μ s	6.3 μ J
SCVR	116.9 ^a nW	19.2 s	2.2 μ J
• μ P+SRAM	90.0 nW	19.2 s	1.7 μ J
Standby Mode	Power	Time/Day	Energy/Day
CDC	172.8 pW	24 hr	14.9 μ J
TRx	3.3 nW	24 hr	285.1 μ J
SCVR	174.8 ^b pW	24 hr	15.1 μ J
• μ P+SRAM	9.8 pW	24 hr	846.7 nJ
• WUC	62.0 pW	24 hr	5.2 μ J

^aIncludes μ P and SRAM power

^bIncludes μ P, SRAM, and WUC power

While these conditions are not typical, in indoor lighting with light irradiance of $15 \mu\text{W}/\text{cm}^2$, V_{SOLAR} drops to near 460 mV and the battery is still recharged with 13 nW, more than offsetting the 5.3 nW monitor's power consumption. The IOPM requires 10 hours of indoor lighting or 1.5 hours of sunlight per day to achieve energy-autonomy. In the latter scenario, the 459 μJ energy required by the microsystem is harvested in 1.5 hours at a rate of 80 nW. Energy-autonomy makes the IOP monitor lifetime decades or longer, giving doctor's ample time tailor a patient-specific glaucoma treatment.

VI. CONCLUSION

A 1.5 mm^3 microsystem, targeted for minimally invasive implantation, measures IOP with an accuracy of 0.5 mmHg. Based on in vivo measurements, the transmitter wirelessly transmits measured pressure data through animal tissue to an external wand. It is designed to transmit data from within the eye to an external wand while consuming 4.7 nJ/bit, providing rapid IOP feedback to decrease physician response time for improved treatment. It harvests up to 80 nW of solar power in

TABLE III
PERFORMANCE SUMMARY OF PREVIOUS WORKS IN DC-DC VOLTAGE CONVERSION

Reference	Method	Efficiency	Power	V_{IN}	V_{OUT}
This Work	SCVR	75%	90nW	3.6V	450mV
This Work	SCVR	40%	72pW	3.6V	450mV
[57]	SC-CP	60%	1.2mW	80mV	500mV
[51]	Boost	80%	100 μ W	250mV	1V
[51]	Boost	45%	1 μ W	250mV	1V
[52]	SCVR	84%	1mW	1.15V	2.1V
[52]	SCVR	10%	1 μ W	1.15V	2.1V
[33]	SCVR	40%	958nW	865mV	3.6V
[53]	Buck	80%	1 μ W	1.2V	500mV
[29]	SCVR	76%	100 μ W	1.2V	500mV
[29]	SCVR	60%	1 μ W	1.2V	500mV
[48]	Hybrid	55%	126nW	3.6V	444mV
[33]	Hybrid	41%	100nW	3.6V	400mV
[33]	Hybrid	18%	100pW	3.6V	400mV

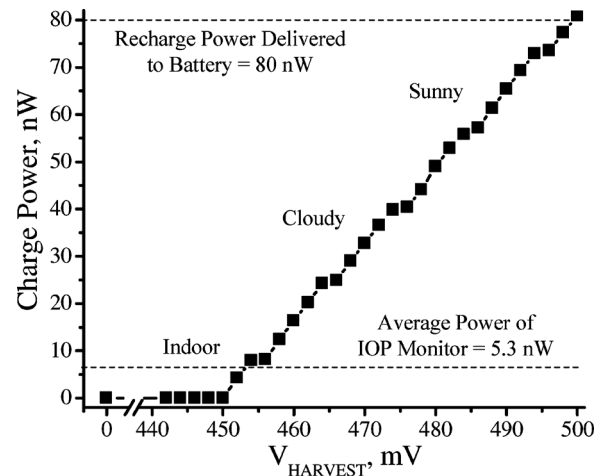


Fig. 14. The solar cells and switched capacitor voltage regulator deliver of power to recharge the battery.

sunlight with a light irradiance of $100 \text{ mW}/\text{cm}^2$ AM 1.5 and uses ultra-low-power circuit techniques to achieve energy autonomy, extending lifetime indefinitely and potentially giving doctors time to converge upon the best glaucoma treatment. Energy-autonomous and nanowatt circuit techniques are needed to the enable cubic-millimeter microsystems that could eventually be used as part of future medical implants, such as blood pressure and glucose sensors, as well as non-medical devices, such as supply chain and infrastructure monitors.

REFERENCES

- [1] H. A. Quigley and A. T. Broman, "The number of people with glaucoma worldwide in 2010 and 2020," *Brit. J. Ophthalmol.*, vol. 90, pp. 262–267, Mar. 2006.
- [2] K. C. Katuri, S. Asrani, and M. K. Ramasubramanian, "Intraocular pressure monitoring sensors," *IEEE Sensors J.*, vol. 8, no. 1, pp. 12–19, Jan. 2008.
- [3] M. Karmel, "The question of IOP," *Eyenet Mag., Amer. Acad. Ophthalmol.*, pp. 39–43, Jun. 2011.

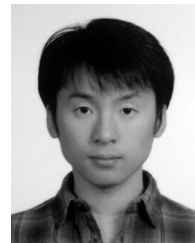
- [4] K. Stangel, S. Kolnsberg, D. Hammerschmidt, B. J. Hosticka, H. K. Trieu, and W. Mokwa, "A programmable intraocular CMOS pressure sensor system implant," *IEEE J. Solid State Circuits*, vol. 36, no. 7, pp. 1094–1100, Jul. 2001.
- [5] Y.-C. Shih, T. Shen, and B. Otis, "A 2.3 μ W wireless intraocular pressure/temperature monitor," in *Proc. IEEE Asian Solid State Circuits Conf.*, Nov. 2010.
- [6] P. Wong, C. Kania, M. Shah, M. R. Moinot, J. Schesser, W. C. Hunter, and T. L. Alvarez, "Interfacing a tonometer with a microcontroller to monitor diurnal intraocular pressure variations," in *Proc. IEEE North-east Bioeng. Conf.*, Mar. 2010.
- [7] M. Leonardi, P. Leuenberger, D. Bertrand, A. Bertsch, and P. Renaud, "A soft contact lens with a MEMS strain gage embedded for intraocular pressure monitoring," in *Proc. IEEE Int. Conf. Transducers, Solid-State Sensors, Actuators, Microsyst.*, Jun. 2003, vol. 2, pp. 1043–1046.
- [8] E. Y. Chow, S. Chakraborty, W. J. Chappell, and P. P. Irazoqui, "Mixed-signal integrated circuits for self-contained sub-cubic millimeter biomedical implants," in *IEEE Int. Solid-State Circuits Conf.*, Feb. 2010, pp. 236–237.
- [9] R. M. Haque and K. D. Wise, "A 3D implantable microsystem for intraocular pressure monitoring using a glass-in-silicon reflow process," in *Proc. IEEE Int. Conf. Micro Electro Mech. Syst.*, Jan. 2011, pp. 995–998.
- [10] R. Haque and K. Wise, "Method of embedding material in a glass substrate," U.S. Patent Application 12/581 695, Oct. 19, 2009.
- [11] R. Haque, K. Wise, and P. Lichter, "Implantable device and surgical implantation technique," U.S. Patent Application 13/154,291, Jun. 6, 2011.
- [12] D. G. Janagama and R. R. Tummala, *Nanobiosensing Electronics and Nanochemistry for Biosensor Packaging*. New York: Springer, 2010, pp. 613–663.
- [13] P.-J. Chen, D. C. Rodger, S. Saati, M. S. Humayun, and Y.-C. Tai, "Microfabricated implantable parylene-based wireless passive intraocular pressure sensors," *IEEE J. Microelectromech. Syst.*, vol. 17, no. 6, pp. 1342–1351, Dec. 2008.
- [14] K. Tanaka, Y. Kuramochi, T. Kurashina, K. Okada, and A. Matsuzawa, "A 0.026 mm² capacitance-to-digital converter for biotelemetry applications using a charge redistribution technique," in *Proc. IEEE Asian Solid-State Circuits Conf.*, Nov. 2007, pp. 244–247.
- [15] M. van Elzaker, E. van Tuijl, P. Geraedts, D. Schinkel, E. A. M. Klumperink, and B. Nauta, "A 10-bit charge-redistribution ADC consuming 1.9 μ W at 1 MS/s," *IEEE J. Solid-State Circuits*, vol. 45, no. 5, pp. 1007–1015, May 2010.
- [16] J. O'Dowd, A. Callanan, G. Banarie, and E. Company-Bosch, "Capacitive sensor interfacing using sigma-delta techniques," in *Proc. IEEE Sensors*, Nov. 2005, pp. 951–954.
- [17] M. Bingesser, T. Loeliger, W. Hinn, J. Hauer, and S. Modl, "Low-noise sigma-delta capacitance-to-digital converter for sub-pF capacitive sensors with integrated dielectric loss measurement," *Proc. Design, Autom., Test Eur.*, pp. 868–872, Mar. 2008.
- [18] B. George and V. J. Kumar, "Analysis of the switched-capacitor dual-slope capacitance-to-digital converter," *IEEE Trans. Instrum. Meas.*, vol. 59, no. 5, pp. 997–1006, May 2010.
- [19] Y. Chae and G. Han, "A low power sigma-delta modulator using class-C inverter," in *Proc. IEEE Symp. VLSI Circuits*, Jun. 2007, pp. 240–241.
- [20] S. Naraghi, M. Courcy, and M. P. Flynn, "A 9 b 14 μ W 0.06 mm² PPM ADC in 90 nm digital CMOS," in *Proc. IEEE Int. Solid-State Circuits Conf.*, Feb. 2009, pp. 168–169.
- [21] D. G. Vaughn, T. Asbury, and P. Riordan-Eva, *General Ophthalmology*, 15th ed. Stamford, CT, USA: Appleton & Lange, 1999.
- [22] R. M. Haque and K. D. Wise, "An intraocular pressure sensor based on a glass reflow process," in *Proc. Solid-State Sensors, Actuators, Microsyst. Workshop*, Jun. 2010, pp. 49–52.
- [23] M. Shafahi and K. Vafai, "Human eye response to thermal disturbances," *ASME J. Heat Transfer*, vol. 133, pp. 011009-1–011009-7, 2010.
- [24] Y. Lin, D. Sylvester, and D. Blaauw, "An ultra low power 1 V, 220 nW temperature sensor for passive wireless applications," in *Proc. Custom Integr. Circuits Conf.*, Sep. 2008, pp. 507–510.
- [25] D. Kim, G. Chen, Y. Lin, D. Fick, J. Park, M. Seok, M. Chen, Z. Foo, D. Blaauw, and D. Sylvester, "A millimeter-scale energy-autonomous sensor system with stacked battery and solar cells," *J. Solid-State Circuits*, vol. 48, no. 3, pp. 801–813, Mar. 2013.
- [26] A. Wang, A. P. Chandrakasan, and S. V. Kosonocky, "Optimal supply and threshold scaling for subthreshold CMOS circuits," in *Proc. IEEE Comput. Soc. Annu. Symp. VLSI*, Apr. 2002, pp. 5–9.
- [27] B. H. Calhoun and A. Chandrakasan, "Characterizing and modeling minimum energy operation for subthreshold circuits," in *Proc. Int. Symp. Low Power Electron. Design*, 2004, pp. 90–95.
- [28] B. Zhai, D. Blaauw, D. Sylvester, and K. Flautner, "Theoretical and practical limits of dynamic voltage scaling," in *Proc. 41st Annu. Design Autom. Conf.*, Jun. 2004, vol. 873, p. 868.
- [29] J. Kwong, Y. K. Ramadass, N. Verma, and A. P. Chandrakasan, "A 65 nm sub-Vt microcontroller with integrated SRAM and switched capacitor DC-DC converter," *IEEE J. Solid-State Circuits*, vol. 44, no. 1, pp. 115–126, Jan. 2009.
- [30] S. C. Jocke, J. F. Bolus, S. N. Wooters, A. D. Jurik, A. C. Weaver, T. N. Blalock, and B. H. Calhoun, "A 2.6- μ W sub-threshold mixed-signal ECG SoC," in *Proc. Symp. VLSI Circuits*, Jun. 2009, pp. 60–61.
- [31] S. Hanson, M. Seok, Y.-S. Lin, Z. Y. Foo, D. Kim, Y. Lee, N. Liu, D. Sylvester, and D. Blaauw, "A low-voltage processor for sensing applications with picowatt standby mode," *IEEE J. Solid-State Circuits*, vol. 44, no. 4, pp. 1145–1155, Apr. 2009.
- [32] M. Seok, D. Sylvester, and D. Blaauw, "Optimal technology selection for minimizing energy and variability in low voltage applications," in *Proc. Int. Symp. Low Power Electron. Design*, Aug. 2008, pp. 9–14.
- [33] G. Chen, M. Fojtik, D. Kim, D. Fick, J. Park, M. Seok, M.-T. Chen, Z. Foo, D. Sylvester, and D. Blaauw, "A millimeter-scale nearly-perpetual sensor system with stacked battery and solar cells," in *Proc. IEEE Int. Solid-State Circuits Conf.*, Feb. 2010, pp. 288–289.
- [34] J. Raszka, M. Advani, V. Tiwari, L. Varisco, N. D. Hacobian, A. Mittal, M. Han, A. Shirdel, and A. Shubut, "Embedded flash memory for security applications in a 0.13 μ m CMOS logic process," in *Proc. IEEE Int. Solid-State Circuits Conf.*, Feb. 2004.
- [35] G. Chen, D. Sylvester, D. Blaauw, and T. Mudge, "Yield-driven near-threshold SRAM," in *Proc. IEEE/ACM Int. Conf. Comput. Aided Design*, Nov. 2007, pp. 660–666.
- [36] L. Chang, Y. Nakamura, R. K. Montoye, J. Sawada, A. K. Martin, K. Kinoshita, F. H. Gebara, K. B. Agarwal, D. J. Acharyya, W. Haensch, K. Hosokawa, and D. Jamsek, "A 5.3 GHz 8T-SRAM with operation down to 0.41 V in 65 nm CMOS," in *Proc. IEEE Symp. VLSI Circuits*, Jun. 2007, pp. 252–253.
- [37] N. Verma and A. P. Chandrakasan, "A 65 nm 8T sub-Vt SRAM employing sense-amplifier redundancy," in *Proc. IEEE Int. Solid-State Circuits Conf.*, Feb. 2007, pp. 328–329.
- [38] B. H. Calhoun and A. Chandrakasan, "A 256 kb Sub-threshold SRAM in 65 nm CMOS," in *Proc. IEEE Int. Solid-State Circuits Conf.*, Feb. 2006, pp. 259–260.
- [39] I. J. Chang, J.-J. Kim, S. P. Park, and K. Roy, "A 32 kb 10T sub-threshold SRAM array with bit-interleaving and differential read scheme in 90 nm CMOS," in *Proc. IEEE Int. Solid-State Circuits Conf.*, Feb. 2008, pp. 388–389.
- [40] D. Kim, G. Chen, M. Fojtik, M. Seok, D. Blaauw, and D. Sylvester, "A 1.85 fW/bit ultra-low leakage 10T SRAM with speed compensation scheme," in *Proc. IEEE Int. Symp. Circuits Syst.*, 2011.
- [41] S. Mandal and R. Sarpeshka, "Power-efficient impedance-modulation wireless data links for biomedical implants," *IEEE Trans. Biomed. Circuits Syst.*, vol. 2, no. 4, pp. 301–315, Dec. 2008.
- [42] G. Wang, W. Liu, M. Sivaprakasam, and G. A. Kendir, "Design and analysis of an adaptive transcutaneous power telemetry for biomedical implants," *IEEE Trans. Circuits Syst. I, Reg. Papers*, vol. 52, no. 10, pp. 2109–2117, Oct. 2005.
- [43] A. C.-W. Wong, D. McDonagh, G. Kathiresan, O. C. Omeni, O. El-Jamaly, T. C.-K. Chan, P. Paddan, and A. J. Burdett, "A 1 V, micropower system-on-chip for vital-sign monitoring in wireless body sensor networks," in *Proc. IEEE Int. Solid-State Circuits Conf.*, Feb. 2008, pp. 138–139.
- [44] Y.-S. Lin, D. Sylvester, and D. Blaauw, "Near-field communication using phase-locking and pulse signaling for millimeter-scale systems," in *Proc. IEEE Custom Integr. Circuits Conf.*, Sep. 2009, pp. 563–566.
- [45] X. Huang, B. Ao, P. Harpe, G. Dolmans, H. Groot, and J. Long, "A 915 MHz 120 μ W-RX/900 μ W-TX envelope detection transceiver with 20 dB in-band interference tolerance," in *Proc. IEEE Int. Solid-State Circuits Conf.*, Feb. 2012, pp. 454–456.
- [46] J. Choi, K. Lee, S. Yun, S. Lee, and J. Ko, "An interference-aware 5.8 GHz wake-up radio for ETCS," in *Proc. IEEE Int. Solid-State Circuits Conf.*, Feb. 2012, pp. 446–448.
- [47] A. Goel and H. Hashemi, "Frequency switching in dual-resonance oscillators," *IEEE J. Solid-State Circuits*, vol. 42, no. 3, pp. 571–582, Mar. 2007.
- [48] M. Wiecekowski, G. K. Chen, M. Seok, D. Sylvester, and D. Blaauw, "A hybrid DC-DC converter for nanoampere sub-1 V implantable applications," in *Proc. IEEE Symp. VLSI Circuits*, Jun. 2009, pp. 166–167.

- [49] M. H. Ghaed, D. Sylvester, and D. Blaauw, "A dual-passband filter architecture for dual-band systems," in *Proc. IEEE Int. Symp. Antennas Propag.*, Jul. 2011.
- [50] V. Raghunathan, A. Kansal, J. Hsu, J. Friedman, and M. Srivastava, "Design considerations for solar energy harvesting wireless embedded systems," in *Proc. Int. Symp. Inf. Process. Sensor Netw.*, Apr. 2005, pp. 457–462.
- [51] E. Carlson, K. Strunz, and B. Otis, "20 mV input boost converter for thermoelectric energy harvesting," in *Proc. IEEE Symp. VLSI Circuits*, Jun. 2009, pp. 162–163.
- [52] M. D. Seeman, S. R. Sanders, and J. M. Rabaey, "An ultra-low-power power management IC for energy-scavenged wireless sensor nodes," in *IEEE Power Electronics Specialists Conf.*, Jun. 2008, pp. 925–931.
- [53] Y. K. Ramadass and A. P. Chandrakasan, "Minimum energy tracking loop with embedded DC-DC converter enabling ultra-low-voltage operation down to 250 mV in 65 nm CMOS," *IEEE J. Solid-State Circuits*, vol. 43, no. 1, pp. 256–265, Jan. 2008.
- [54] *Cymbet Corporation Rechargeable Thin Film Battery 12 μ Ah 3.8 V Datasheet.*, Elk River, MN, USA, Cymbet Corp..
- [55] *Infinite Power Solutions Rechargeable Thin Film Battery Thin Energy MEC-120 Datasheet.* Littleton, CO, USA: Infinite Power Solutions.
- [56] *Standard Tables for Reference Solar Spectral Irradiances* ASTM International, West Conohocken, PA, USA, 2003, American Society of Testing and Materials Standard G173-03.
- [57] X. Zhang, K. Ishida, Y. Okuma, Y. Ryu, M. Takamiya, and T. S. P. Chen, "An 80 mV startup dual-mode boost converter by charge-pumped pulse generator and threshold voltage tuned oscillator with hot carrier injection," *J. Solid-State Circuits*, vol. 47, no. 11, pp. 2554–2562, Nov. 2012.

Dr. Haque is currently the President & CEO of Structured Microsystems LLC, a spinoff from the University of Michigan that is specializing in microsystem design and especially on products based on the proprietary glass-in-silicon reflow process that he developed during his graduate work. His main area of interest is in implantable BioMEMS and novel microfabrication techniques that enable new microsystems for interdisciplinary solutions.



Michael Wieckowski received the Ph.D. degree in electrical and computer engineering from the University of Rochester, NY, in 2007. In 2008 he became a Postdoctoral Research Fellow at the University of Michigan, Ann Arbor. His work is focused on low-power mixed-signal design to enable energy constrained computing platforms. He is currently with Mala Geosciences, Charleston, SC.



Yejoong Kim received the B.S. degree in electrical engineering from Yonsei University, Seoul, Korea, in 2008, and the M.S. degree in electrical engineering and computer science from the University of Michigan, Ann Arbor, MI, in 2012. He is currently working toward the Ph.D. degree at the University of Michigan, Ann Arbor. His research interests include subthreshold circuit designs, ultra low-power SRAM, and the design of millimeter-scale computing systems and sensor platforms.

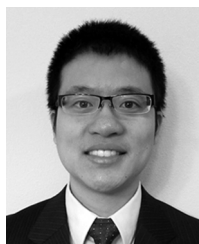


Mohammad Hassan Ghaed (S'08) received the B.S. degree in electrical engineering from Sharif University of Technology, Tehran, Iran, in 2008, and the M.S. degree in electrical engineering from the University of Michigan, Ann Arbor, in 2008, where he is currently working towards the Ph.D. degree.

As a Ph.D. student he was the recipient of Horace H. Rackham graduate fellowship. In summer 2012, he held a research intern position with Rambus Corp, Sunnyvale, CA. His current research interests include analog, mixed signal, and RF-IC design.



Gyouho Kim received the B.S. and M.S. degrees in electrical engineering from the University of Michigan, Ann Arbor, in 2009 and 2011, respectively, where he is currently pursuing the Ph.D. degree in electrical engineering. His research interests include ultra-low power VLSI design for energy-constrained systems.



Greg Chen (S'06–M'11) received the B.S., M.S., and Ph.D. degrees in electrical engineering from the University of Michigan in 2006 and 2009, and 2011. He currently is a member of the High-Performance Circuits research group at Intel, Hillsboro, OR. His research interests include networks-on-chip and low-power circuits.



Yoonmyung Lee (S'08–M'12) received the B.S. degree in electronic and electrical engineering from the Pohang University of Science and Technology (POSTECH), Pohang, Korea, in 2004, and the M.S. and Ph.D. degrees in electrical engineering from the University of Michigan, Ann Arbor, in 2008 and 2012, respectively. He is currently a research fellow at the University of Michigan, where he researches energy-efficient ultra-low power integrated circuits for low-power high-performance VLSI systems and millimeter-scale wireless sensor systems.

Dr. Lee was a recipient of Samsung Scholarship and Intel Ph.D. fellowship.



Razi-ul Haque received B.S.E. degrees in both Electrical Engineering and Computer Engineering from the University of Michigan, Ann Arbor in 2004. He received the M.S.E. degree in Electrical Engineering in 2005 and a Ph.D. in Electrical Engineering: Circuits & Microsystems in 2011, all from the University of Michigan, Ann Arbor. Since 2001, he has worked on a variety of microelectromechanical systems, from microfluidic devices for DNA analysis to a highly-integrated and compact microsystem for in-vivo continuous monitoring.

During his postdoctoral work at the University of Michigan, he explored neural probe designs that reduced neural tissue damage by minimizing silicon area.



Inhee Lee (S'07) received the B.S. and the M.S. degrees in electrical and electronic engineering from Yonsei University, Seoul, Korea, in 2006 and 2008, respectively. He is pursuing the Ph.D. degree in University of Michigan, Ann Arbor. His current research interest includes a low-power sigma-delta modulator, a low-power capacitive energy harvester, a low-power battery supervisory circuit and a micro-scale wireless sensor node.



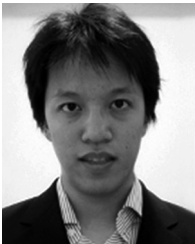
David Fick (S'08–M'10) received the B.S.E. degree in computer engineering (2006), the M.S.E. in computer science and engineering (2009), and the Ph.D. in computer science and engineering (2012), all from the University of Michigan. He is currently a Research Associate at the Michigan Integrated Circuits Lab (MICL). He has authored three patents and published more than a dozen papers. His research interests include fault tolerance, adaptive circuits and systems, and 3D integrated circuits.



Daeyeon Kim (S'08) received the B.S. degree in electronic and electrical engineering from Pohang University of Science and Technology (POSTECH), Pohang, Korea, in 2006, and the M.S. and Ph.D. degrees in electrical engineering from the University of Michigan, Ann Arbor, in 2008 and 2012, respectively. He was a graduate research intern at ARM, Inc., in 2010 and 2011. After finishing the Ph.D. in 2012, he joined Advanced Design Group, Logic Technology Development, Intel Corporation, Hillsboro, OR 94124 USA where he works on

low-power high-performance SRAM design, statistical yield analysis, and process variation mitigation techniques.

Dr. Kim received a best paper award at International Symposium on Low Power Electronics and Design in 2009.



Mingoo Seok (S'05–M'11) is an assistant professor in the Department of Electrical Engineering, School of Engineering and Applied Science at Columbia University since 2012. He received the B.S. (with summa cum laude) in electrical engineering from Seoul National University, South Korea, in 2005, and the M.S. and Ph.D. degree from University of Michigan in 2007 and 2011, respectively, all in electrical engineering. He has spent about a year as a member of technical staff in the Systems and Applications R&D Center of Texas Instruments,

Dallas, TX. He has a research interest in energy-efficient and high performance integrated circuit and system design for cyber physical systems, mobile electronics, and cloud computing platforms. He received 1999 Distinguished Undergraduate Scholarship from the Korea Foundation for Advanced Studies, 2005 Doctoral Fellowship from the same organization, and 2008 Rackham Pre-Doctoral Fellowship from University of Michigan, Ann Arbor. He also won 2009 AMD/CICC Scholarship Award for picowatt voltage reference work and 2009 DAC/ISSCC Design Contest for the 35pW sensor platform design (a.k.a. Phoenix Processor). He holds one pending international patent.



Kensall D. Wise (S'61–M'69–SM'83–F'86–LF'07) received the B.S.E.E. degree with highest distinction from Purdue University in 1963 and the M.S. and Ph.D. degrees in electrical engineering from Stanford University in 1964 and 1969, respectively. From 1963 to 1965 and from 1972 to 1974, he was a Member of Technical Staff at Bell Telephone Laboratories, where his work focused on the exploratory development of integrated electronics for use in telephone communications. From 1965 to 1972 he was a Research Assistant and then a Research Associate and Lecturer at Stanford, working on the development of micromachined solid-state sensors. In 1974 he joined the University of Michigan, Ann Arbor, where he is now the William Gould Dow Distinguished University Professor Emeritus of Electrical Engineering and Computer Science. Dr. Wise was

General Chairman of the 1984 IEEE Solid-State Sensor Conference (Hilton Head) and was Technical Program Chairman (1985) and General Chairman (1997) of the IEEE International Conference on Solid-State Sensors, Actuators, and Microsystems. He received the 1990 Paul Rappaport Award from the IEEE Electron Devices Society, the 1995 Distinguished Faculty Achievement Award from the University of Michigan, the 1996 Columbus Prize from the Christopher Columbus Fellowship Foundation, the 1997 SRC Aristotle Award, and the 1999 IEEE Solid-State Circuits Technical Field Award. He held the 2007 Henry Russel Lectureship at the University of Michigan and is a Life Fellow of the IEEE, a Fellow of the AIMBE, and a member of the United States National Academy of Engineering.



David Blaauw (M'94–SM'07–F'12) received the B.S. degree in physics and computer science from Duke University in 1986, and the Ph.D. degree in computer science from the University of Illinois, Urbana, in 1991. Until August 2001, he worked for Motorola, Inc., in Austin, TX, where he was the manager of the High Performance Design Technology group. Since August 2001, he has been on the faculty at the University of Michigan where he is a Professor. He has published over 350 papers and hold 40 patents. His work has focussed on VLSI

design with particular emphasis on ultra low power and high performance design.

Dr. Blaauw was the Technical Program Chair and General Chair for the International Symposium on Low Power Electronic and Design. He was also the Technical Program Co-Chair of the ACM/IEEE Design Automation Conference and a member of the ISSCC Technical Program Committee. He is an IEEE Fellow.



Dennis Sylvester (S'95–M'00–SM'04–F'11) received the Ph.D. degree in electrical engineering from the University of California, Berkeley, where his dissertation was recognized with the David J. Sakrison Memorial Prize as the most outstanding research in the UC-Berkeley EECS department. He is a Professor of Electrical Engineering and Computer Science at the University of Michigan, Ann Arbor and Director of the Michigan Integrated Circuits Laboratory (MICL), a group of ten faculty and 60+ graduate students. He previously held

research staff positions in the Advanced Technology Group of Synopsys, Mountain View, CA, Hewlett-Packard Laboratories in Palo Alto, CA, and a visiting professorship in electrical and computer engineering at the National University of Singapore. He has published over 300 articles along with one book and several book chapters. His research interests include the design of millimeter-scale computing systems and energy efficient near-threshold computing for a range of applications. He holds 12 US patents. He also serves as a consultant and technical advisory board member for electronic design automation and semiconductor firms in these areas. He co-founded Ambiq Micro, a fabless semiconductor company developing ultra-low power mixed-signal solutions for compact wireless devices.

Dr. Sylvester received an NSF CAREER award, the Beatrice Winner Award at ISSCC, an IBM Faculty Award, an SRC Inventor Recognition Award, and eight best paper awards and nominations. He is the recipient of the ACM SIGDA Outstanding New Faculty Award and the University of Michigan Henry Russel Award for distinguished scholarship. He has served on the technical program committee of major design automation and circuit design conferences, the executive committee of the ACM/IEEE Design Automation Conference, and the steering committee of the ACM/IEEE International Symposium on Physical Design. He has served as Associate Editor for IEEE TRANSACTIONS ON COMPUTER-AIDED DESIGN OF INTEGRATED CIRCUITS AND SYSTEMS and IEEE TRANSACTIONS ON VERY LARGE SCALE INTEGRATION (VLSI) SYSTEMS